THE 4TH INTERNATIONAL CONFERENCE ON ALUMINUM ALLOYS

THE DEVELOPMENT OF MICROSTRUCTURE IN 6000 SERIES ALUMINUM SHEET FOR AUTOMOTIVE OUTER BODY PANEL APPLICATIONS

A.K. Gupta, G.B. Burger, P.W. Jeffrey and D.J. Lloyd

Alcan International Limited, Kingston Research and Development Centre
Box 8400, 945 Princess Street, Kingston, Ontario, K7L 5L9

Introduction

The introduction of new materials in the automotive industry is being driven by a variety of techno-economic issues[1], but the main result is a drive towards weight reduction. The replacement of steel sheet by aluminum alloys can provide a direct body-in-white weight reduction of up to about 47%, and further secondary weight savings can be realized because the lower loads will permit lighter components in the rest of the vehicle without loss of performance.

The basic requirement for automotive sheet is to have a high formability so that the panels can be stamped while retaining, or preferably increasing its strength when the part is painted and thermally cured. Two types of aluminum alloys are being used: the non-heat treatable Al-Mg alloys of the 5000 series, and the heat treatable Al-Cu, Al-Mg-Si and Al-Mg-Si-Cu of the 2000 and 6000 series. The 5000 series alloys have very good formability, but relatively low strength, and are generally used for interior, structural applications. The heat treatable alloys have higher strength, and hardening during the paint bake cycle, and are used for automotive skins where dent resistance is important. The 2000 series have been the most extensively used alloys, particularly AA2008 and AA2036 which have been used, respectively, for the inner and outer hoods of the Lincoln Towncar for many years. However, they have a low paint bake hardenability at the present paint bake temperatures, and this puts them at a strength disadvantage relative to the 6000 series alloys.

This paper will consider the microstructure-property relationships in the 6000 series alloys which are relevant to automotive applications.

Commercial Processing

The alloys are cast as ingots, typically 610 mm thick, and to a width and length dependent upon both the final product as well as the capability of the processing equipment (such as rolling mills, furnaces, etc.). The ingots are scalped on their rolling surfaces to remove physical irregularities and a thin layer of inverse segregation. In preparation for hot rolling, the ingots are preheated to a temperature of over 500°C, in a cycle often as long as 24 hours, which also serves to homogenize much of the coring (short range intercellular segregation) and to dissolve any of the soluble phases in the ingot. The ingots are then introduced to the hot rolling line. The line typically consists of a 4-high reversing mill which serves to break down the ingot into a slab, and a high speed multi-stand tandem line which reduces the slab to coilable strip at a gauge between 2 and 5 mm (referred to as reroll). Following this, the

coils are allowed to cool before they are cold rolled to the final gauge. For 6000 series skin sheet products the final gauge is typically between 0.9 and 1.2 mm. The sheet is then solution treated in order to obtain the optimum formability and an age hardening response during the paint bake of the final part. The solution treatment requires a continuous heat treatment line wherein the sheet is unwound from the coil and passed single-strand through the line where it is rapidly heated to a temperature between 500°C and 570°C to dissolve the hardening phases and then quenched to retain the major alloying additions in solid solution. After the final anneal or solution treatment all sheet products are levelled, possibly pretreated for some specific applications and are generally prelubricated before being supplied for blanking and stamping.

6000 Series Alloys

The compositions of some of the automotive 6000 series alloys are given in Table I. The major alloying elements for strength are Mg, Si and Cu, while Mn is sometimes present in limited amounts to provide grain size control. The main strengthening precipitate is Mg_2Si, with additional precipitates of Si in the excess Si alloys, and Q-phase, $Al_5Cu_2Mg_8Si_5$, in the higher Cu alloys.

Table I. Composition of some of the aluminum alloys used for automotive panel applications (weight percent).

Alloy	Mg	Si	Cu	Fe	Mn	Zn	Cr	Ti
5754	2.60–3.60	≤ 0.40	≤ 0.10	≤ 0.40	≤ 0.50	—	≤ 0.30	≤ 0.10
5182	4.0–5.0	0.20	0.15	0.35	0.2–0.5	0.25	0.10	0.10
5030	4.0–5.0	0.08	≤ 0.30	≤ 0.40	≤ 0.10	—	≤ 0.05	0.10
5032	5.0–6.0	0.25	0.50	0.40	0.20	0.10	0.20	0.10
6009	0.4–0.8	0.6–1.0	0.15–0.60	≤ 0.50	0.2–0.8	≤ 0.25	≤ 0.10	≤0.10
6010	0.60–1.0	0.8–1.2	0.15–0.60	≤ 0.50	0.2–0.8	≤ 0.25	≤ 0.10	≤0.10
6111	0.5–1.0	0.6–1.1	0.5–0.9	≤ 0.40	≤ 0.40	—	≤ 0.10	≤ 0.10
6016	0.3–0.6	1.0–1.5	≤ 0.20	≤ 0.50	≤ 0.20	—	0.10	—
2008	0.25–0.50	0.5–0.8	0.7–1.1	≤ 0.40	≤ 0.30	≤ 0.25	≤ 0.10	≤ 0.10
2010	0.40–1.0	0.50	0.7–1.3	≤ 0.50	0.1–0.40	≤ 0.30	≤ 0.15	—
2036	0.3–0.60	≤ 0.50	≤ 2.2	≤ 0.50	0.1–0.40	≤ 0.25	0.10	≤ 0.15

Of the 6000 series alloys, alloys AA6009 and AA6016 have very similar mechanical properties. They have low T4 yield strengths and so exhibit excellent formability, but this is accompanied by a relatively low strength after the paint bake, typically around 180 MPa. Alloy AA6010 has a much higher strength after the paint bake but its T4 yield strength is also very high, which limits this alloy's formability. Alloy AA6111 has a T4 yield strength of 150-170 MPa and a yield strength after the paint bake of over 200 MPa, which provides it with a good combination of initial formability and final strength. In Europe, the high formability of AA6016 has made it the main automotive skin alloy. In North America, AA6111 is the preferred alloy because of its high final strength and hence dent resistance.

Microstructural Development

In the heat treatable alloys, a solution heat treatment step is utilized to promote the age hardening response. This process is carried out at final gauge in the cold-rolled material. Thus recrystallization in the sheet occurs concurrently with the solutionizing step. The microstructural characteristics developed during recrystallization, most notably grain size/shape and crystallographic texture, exert a significant influence on the isotropy of the mechanical properties of the sheet. This becomes an important consideration when forming large sheet components.

The structure of the sheet prior to the final recrystallization stage, both in terms of the size and distribution of secondary phases (precipitates, dispersoids and constituents) and the substructure (i.e. degree of cold work), control the microstructure developed during recrystallization. In some materials, the influence of heating rate can also have a marked effect on the recrystallization process and the resulting microstructure, depending upon the prior processing route taken.

(a)   (b)
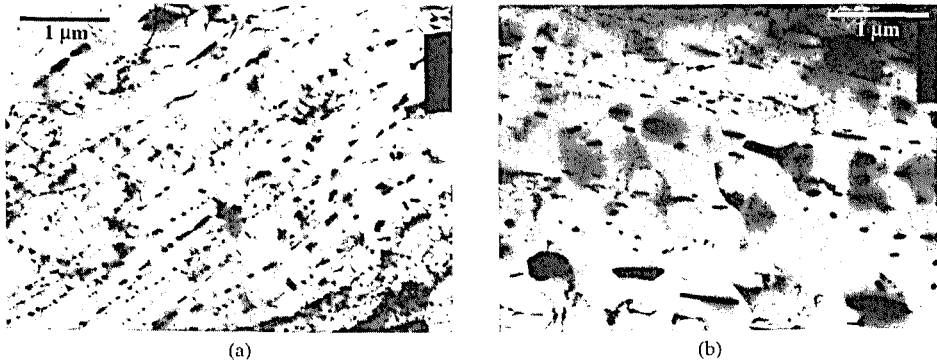
Figure 1:   Precipitate distributions developed through different thermomechanical processing routes, prior to final cold rolling and solution heat treatment.

The limits for the alloying elements which form large constituents (during ingot solidification) and dispersoids (during ingot cooling and homogenization) are set by considerations such as cost, recyclability, and the levels beyond which there are no deleterious effects on mechanical properties. The size, structure and distribution of these second-phase particles is controlled through casting practice, and subsequent thermo-mechanical processing (TMP) schedule. Beyond the effects of these phases in controlling the recrystallization process, there is also the effect of precipitates. It is well known that, in heat-treatable alloys, control over precipitation which occurs throughout the entire TMP schedule can significantly influence the recrystallization behaviour and resulting microstructure[2,3,4]. Relatively minor process changes often produce considerable modifications to the precipitate distribution. This is demonstrated in Figures 1(a) and (b), in which differences in TMP conditions have resulted in major differences in the precipitate distribution.

An example of the influence which the precipitates have in the recrystallization is clearly observed in Figure 2, where the fine scale precipitation inhibits grain boundary migration during recrystallization. Here the cold rolled sheet has been heated to 450°C. The material is fully recrystallized, however temperatures were not high enough to achieve significant solutionizing of the precipitate phases. The precipitation dissolves after recrystallization is complete, at higher temperatures attained in the full solution heat treatment process.
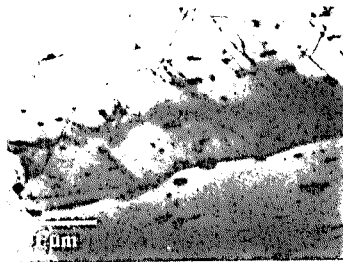
Figure 2:   TEM micrograph of sheet heat treated to 450°C, prior to full solutionizing, illustrating grain boundary pinning by the precipitate phases.

The net effect on the recrystallized microstructure is demonstrated for a 6000 series alloy in the following comparison. Three different processing routes (A, B and C) prior to final solution heat treatment were carried out which develop very different precipitate distributions. The subsequent cold reduction schedule and solution heat treatment practice were maintained invariant for these three cases. The resulting grain structures are given in Figures 3(a), (b) and (c). These range from an elongated grain shape with an average grain intercept length of 40.1 μm in the rolling direction and aspect ratio of 2.4:1 seen in Figure 3(a) (Process A), to a finer elongated grain structure in Figure 3(b) (Process B) with an average grain intercept dimension of 34.4 μm and aspect ratio of 2.3:1 to a more equi-axed grain structure with a grain size of 26.5 μm and aspect ratio of 1.5:1 observed in Figure 3(c) (Process C).

| (a) Process A | (b) Process B | (c) Process C |
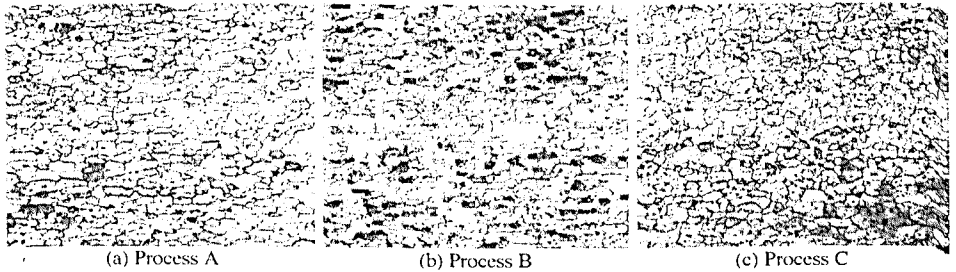
Figure 3: Recrystallized microstructures in a 6000 series alloy after solution heat treatment, produced via three different TMP routes.

The ODF's of the corresponding recrystallized textures are given in Figures 4(a), (b) and (c). These are given as constant ψ_2 sections at $\psi_2 = 0'$. The volume fractions of major texture components have also been calculated from these ODF's utilizing Gaussian model functions with a spread parameter $\varnothing_0 = 11'$. These results are given in Table II. Process C produces sheet with a recrystallized texture containing significantly weaker Goss, S and RX components.

| 0.70 | 1.00 | 1.40 | 2.00 | 2.80 | 4.00 | 5.60 | 8.00 | 11.0 | 16.0 |
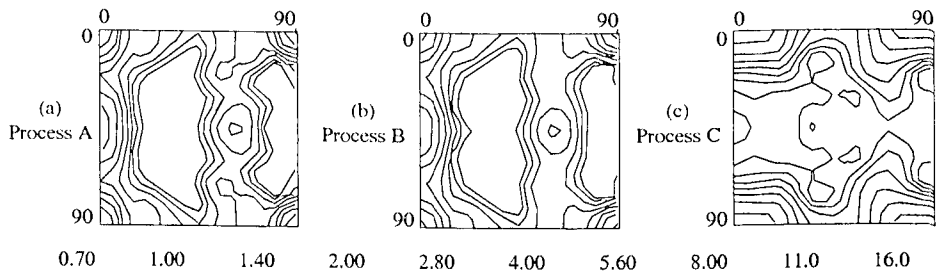
Figure 4: ODF's of recrystallized textures corresponding to microstructures given in Figure 3. Contours are scaled relative to a random texture.

Table II. Calculated volume percentages of major texture components in 6000 series alloy in the T4 condition, processed via three different TMP routes.

Process/ Composition	Cube {001}<100>	Goss {011}<100>	S {123}<634>	RX {011}<8 11 11>
Process A	5.0	3.3	5.2	4.0
Process B	4.1	3.7	6.2	3.8
Process C	4.7	0.6	4.3	2.1

The range of textures produced via these different processing routes is reflected in the subsequent mechanical properties, specifically in the plastic flow behaviour. This is demonstrated in Figure 5, where the predicted and measured R values for each of the materials are presented as a function of orientation in the sheet. The predicted R values were calculated using a full constraints Taylor calculation [5], utilizing the ODF's given in Figure 4. Although there are considerable differences between the predicted and measured R values, the variation with orientation is reasonably well predicted. The differences in R values between the three materials illustrates that the range in microstructures and properties of the sheet which can be produced through control over the recrystallization process, via the influence of the precipitate distribution, can be very significant in some 6000 series alloys.
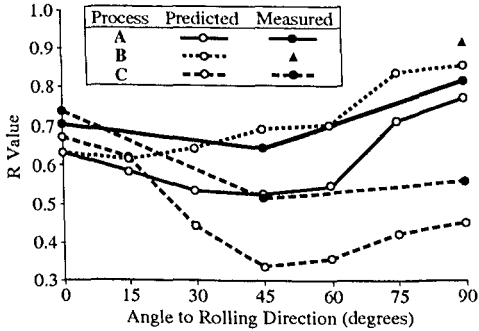
Figure 5: Predicted and measured R values for recrystallized structures given in Figure 3, produced via different TMP routes.
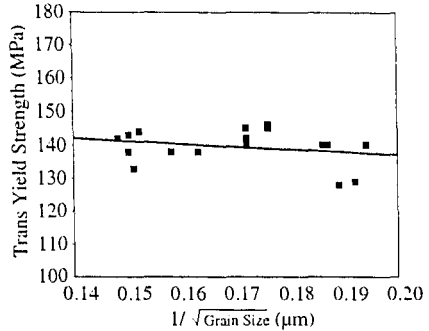
Figure 6: Relationship of yield strength to grain size for a 6000 series alloy in the T4 temper.

These 6000 series alloys show little dependence of the strength upon the grain size over the range which is commercially available at present. This is shown in Figure 6, which is a Petch plot for a 6000 series alloy produced with a range of grain sizes in a fully solution treated state, after a period of natural ageing of approximately one month. It is clear that the yield strength is essentially unchanged over the range of grain size involved (27 to 46 μm). The Petch 'k' parameter of -0.084, considering a tolerance of approximately ± 2 μm on the grain size, shows that this slope is not statistically different from zero.

The frictional stress term in the Petch relation is 153.8 MPa, which is significantly higher than the level usually obtained for Al-Mg alloys (20-60 MPa). This difference is primarily caused by coherent clusters which develop during ambient temperature ageing. Figure 7 is a natural age hardening curve for a solution treated 6000 series
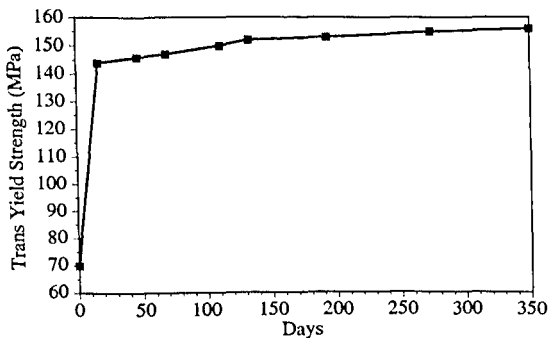
Figure 7: Natural age hardening curve for a solution treated 6000 series alloy.

181

alloy. The intercept at zero time provides the frictional stress of 70 MPa due to the solid solution hardening and to the presence coherent zones formed during quenching, with the difference of 83.9 MPa due to ambient temperature clustering. The ageing curve proceeds in a parabolic manner such that relative stability is achieved after one month, with another 10 MPa being added to the strength on ageing up to one year.

The 6000 series alloys do not exhibit a Lüders elongation during deformation, as is commonly observed in 5000 series alloys in the O-temper condition. This is because of the low Mg content and the fact that the other soluble elements such as Si and Cu are either energetically bound to the Mg in the form of coherent clusters or possess diffusion rates which are too low to enable the formation of effective atmospheres which pin dislocations.

It should be noted that Lüdering is not the only manner of surface roughening which may present a problem with surface-critical products. It is well established that the phenomena of 'orange peeling', if developed during forming, can result in an unsatisfactory surface appearance if the grain size is too large [6]. This is not typically a problem with 5000 series alloys as a grain size of 25 µm largely avoids the issue without making the sheet overly sensitive to Lüdering. Above a grain size of 45 µm the problem can become visually unacceptable, while at the same time there can be a degradation of formability due to early incipient neck formation. Figure 8 illustrates the reduction in level of orange peeling when reducing the grain size from 49 x 17 µm to 31 x 14 µm after a strain of 20%. The orange peel with the finer grain is difficult to resolve visually.

Grain size
49 x 17 µm

Coarse
"orange peel"

Grain size
31 x 14 µm

Fine
"orange peel"

Microstructure in cross section   Surface after 20% strain
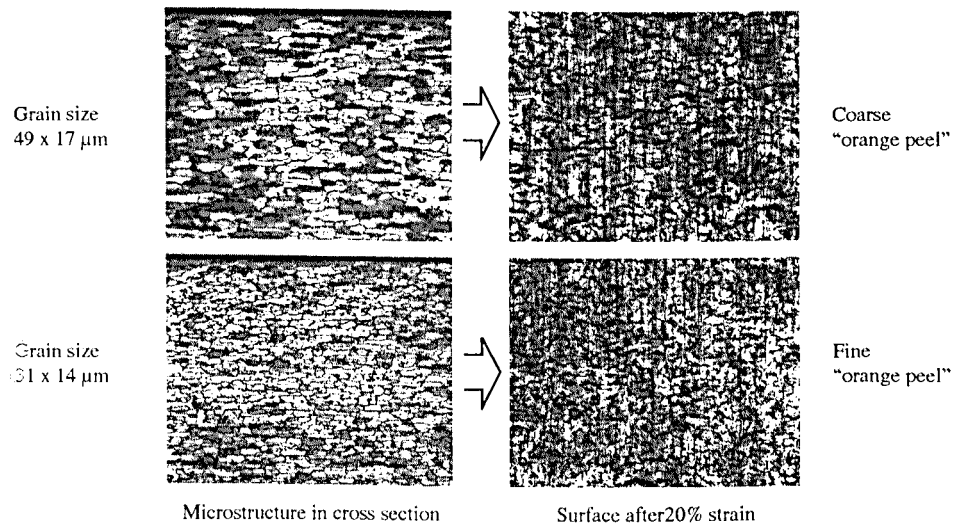
Figure 8: Influence of grain size upon surface "orange peel" after 20% uniaxial strain, illustrating the reduction in surface roughness with decreasing grain size.

While the sheet is recrystallised after the solutionizing, it may not be dislocation "free". Depending on the alloy, the peak metal temperature and the rate of cooling, dislocations may be generated during the "quench". Vacancies may quench out in the form of dislocation loops, or dislocations may be punched out from dispersoid particles as a result of the difference in coefficient of thermal expansion between the dispersoid and the matrix. An example of the latter is shown in Figure 9(a).

The distortion produced in the sheet during cooling from the solutionizing temperature to room temperature requires that the sheet be levelled before going to the customer. The extent of levelling depends on the degree of distortion, but this also results in a significant dislocation density, as seen in Figure 9(b).
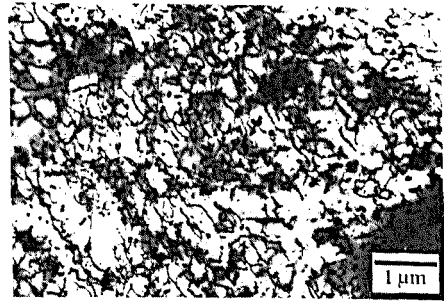
(a) Quenched	(b) Quenched and levelled

Figure 9: Microstructures developed in a solution treated 6000 series alloy after (a) quenching, and (b) quenching and subsequent sheet levelling operations.

<u>Precipitation Sequence</u>

It would be very lengthy, and perhaps not too productive, to discuss the age hardening characteristics of the various 6000 series materials of interest on an alloy-by-alloy basis. It is, however, possible to discuss the general precipitation phenomena in these alloys and how different process variables can change material properties.

Figure 10(a) shows a bright field image of a 6000 alloy in the solution treated state following quenching and natural ageing. The microstructure is relatively clean, except for the presence of quenched-in dislocations and dispersoid particles. The mottled background suggests the presence of coherent zones in the matrix. The mechanical properties are reasonably stable at room temperature and such material is commonly supplied in the T4 temper for stamping into skin panels with subsequent cleaning, painting and curing operations. Figure 10(b) shows a typical microstructure of a material after all these operations. During the stamping additional dislocations are generated while further zones/clusters are formed during the curing process. It should be noted that the shape of the zones at this stage is not clearly visible, although the microstructure corresponds to approximately 50% increase in strength from the T4 temper. The increase in strength is due to the combination of work hardening and precipitation hardening that takes place during forming and paint cure. The latter component is related to the mechanisms and kinetics of the precipitation process which operate during curing.
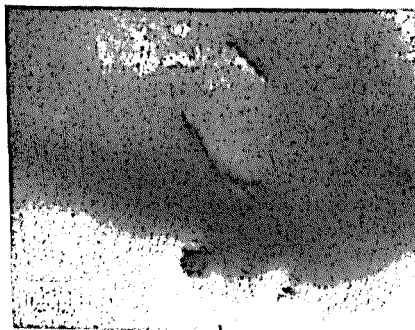
50-80% increase in YS
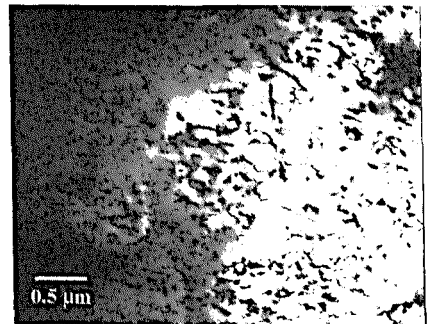
(a) T4 temper	(b) 2% stretch + 0.5 h @ 177°C

Figure 10: Microstructures developed in a solution treated 6000 series alloy (a) in the solution treated state following quenching and natural ageing, and (b) after an applied forming and paint cure simulation.
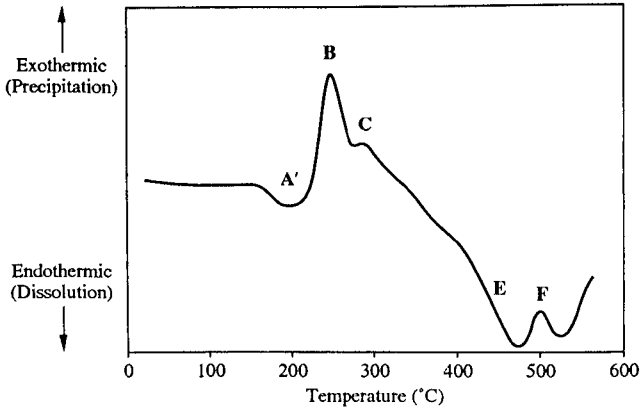
Figure 11: DSC curve of a typical automotive 6000 series skin alloy in the T4 condition.

The precipitation sequence of a typical automotive 6000 skin alloy in T4 condition can be followed from the DSC curve in Figure 11. As the specimen is heated, the peaks and valleys in the curve represent the precipitation and dissolution reactions respectively, while their order of appearance is indicative of the precipitation sequence. The microstructural changes that occur during heating and holding for 15 minutes at different temperatures are superimposed on the DSC curve in Figure 12, specifically for AA6016 in T4 condition. It should be noted that the microstructures shown are not strictly representative of those generated during the actual DSC heating because of the enhanced precipitation caused by the 15 minute soak at each temperature. The precipitation processes associated with different peaks of the curve have been identified. The precipitation sequences that occur during ageing or during linear heating are as follows:
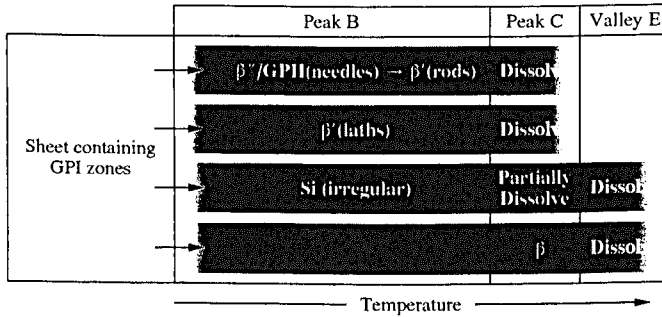
In the freshly solution treated condition the precipitation process begins with the formation of coherent and spherical GP I zones or pre-clusters with no internal order. The alloy used in this study was already in stable T4 temper and contained GP I zones, as supported by the presence of the first dissolution valley A' in the curve shown in Figure 11. As ageing proceeds, the GP I zones become ordered and acquire an acicular or needle shape. At this stage they are called GP II zones [7]. In this study the GP II zones have been equated with the monoclinic transition β" phase, although a few investigators have suggested β" to be a separate phase that forms prior to β' phase [8,9]. At this point in the process precipitation of Si has also been observed. Prolonged ageing results in the transformation of β" needles into semi-coherent β' rods with hexagonal crystal structure, whose axes lie in <100> matrix directions. Some of the β' particles nucleate independently on dislocations and grow as laths on prolonged ageing. The precipitation of β", Si, β' laths and transformation of β" to β' causes the precipitation peak B in the DSC curve of Figure 11 to disappear. At this point the material has passed peak strength and is in an overaged condition,

184
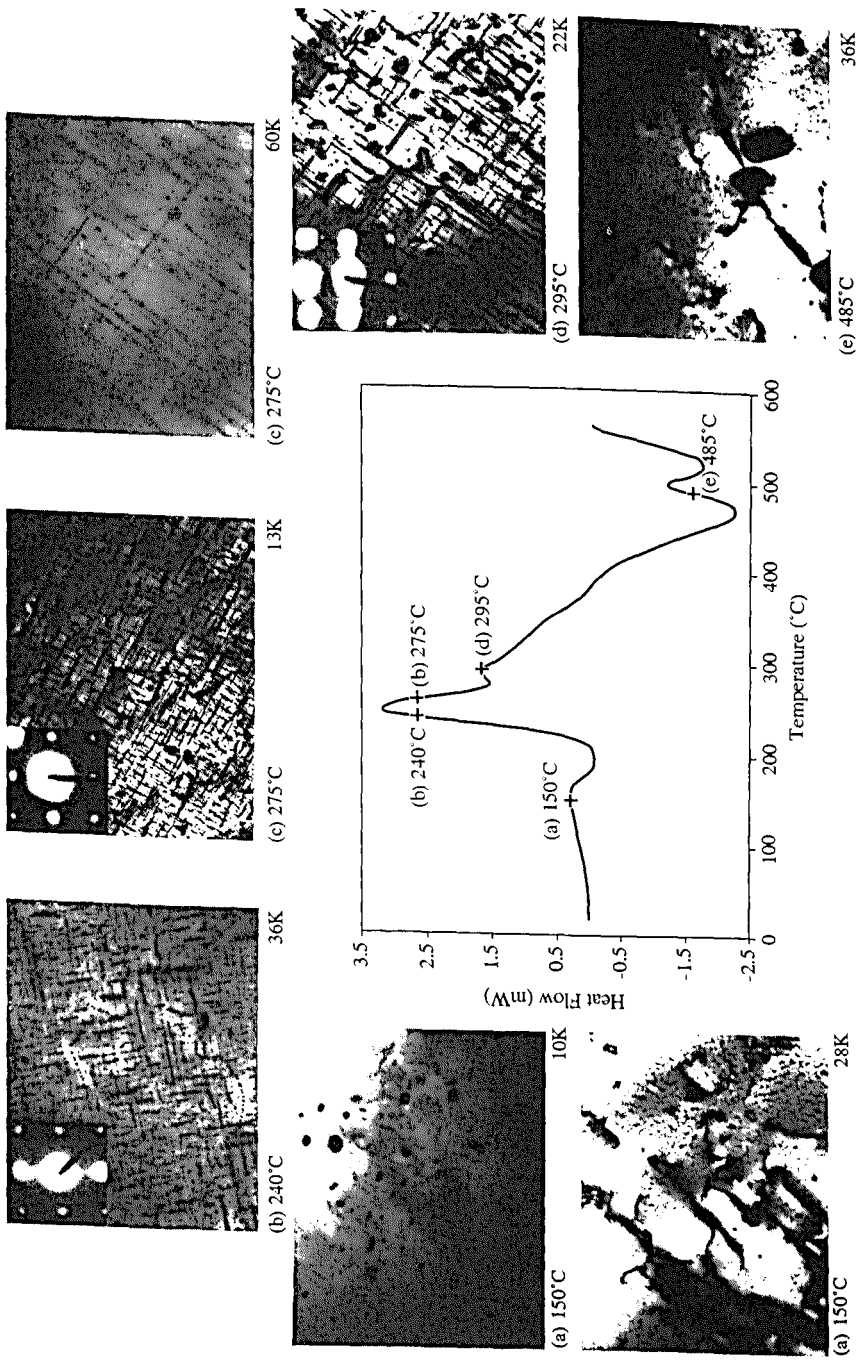
Figure 12: DSC trace of AA6016 in T4 condition, illustrating the development of microstructure associated with specific peaks and valleys on the curve. The microstructures shown were obtained by heating the material at 10°C/min to the temperatures indicated, then holding for 15 minutes and cooling to room temperature.

in which β' loses coherency and starts dissolving, while the equilibrium β (Mg₂Si) phase begins to form independently on the preexisting dispersoids or Si particles.

The precipitation sequence in Al-Mg-Si alloys is usually reported to be continuous, although the results of our work clearly suggest that three different overlapping precipitation sequences are operative. It should be noted that the kinetics of the precipitation processes for the individual sequences, and those associated with the formation of the individual metastable particles, are closely related to the alloy composition and the processing history of the material. The precipitation sequences described here are a signature for a fixed processing route and composition. We have found that the sequences can be altered considerably if either of the two variables are changed. This means that the precipitation process can only be determined on an alloy-by-alloy basis for a fixed processing route.

Summary

To obtain the optimum properties in 6000 series alloys for automotive sheet, all stages of the processing history have to be carefully controlled. By controlling the thermomechanical processing route the size and distribution of dispersoids and soluble precipitates is adjusted to achieve the appropriate grain size, shape and crystallographic texture. The final strength in the formed part is achieved by artificial ageing during the paint bake, and this is a function of alloy. In the commercial alloys the precipitation sequence does not appear to be continuous, but rather involves several precipitation processes operating concurrently. The relative rates at which these processes operate are strongly dependent upon alloy composition, and the processing route. By appropriate choice of alloy and processing, different combinations of formability and strength can be achieved.

References

1. S.A. Arnold, *JOM* (1993), 45, [6], 12.

2. J.A. Wert, N.E. Paton, C.H. Hamilton and M.W. Mahoney, *Met. Trans.*, (1981), 12A, 1267.

3. J.A. Wert and L.K. Austin, *Met. Trans.*, (1988), 19A, 617.

4. M.A. Zaidi and J.A. Wert, in *Aluminum Alloys—Contemporary Research and Applications*, edited by A.K. Vasudevan and R.D. Doherty, Academic Press, San Diego, (1989), 156.

5. P. Van Houtte, *MTM–FHM Software System, Version 1*, (1993).

6. R. Akeret, in *MECAMAT '91*, edited by Teodosiu, Raphanel & Sidoroff, Balkema, Rotterdam, (1993), 195.

7. I. Kovacs, J. Lendvai and E. Nagy, *Acta Met.*, (1972), 20, 975.

8. I. Dutta and S.M. Allen, *J. Mat. Sci. Letters* (1991), 10, 323.

9. H. Westengen and N. Ryum, *Z. Metallkunde*, (1979), 70, 528.